Summer 7-19-2017

# Characterization of a Carbonate Sand based on Shear Wave Velocity Measurement

Abouzar Sadrekarimi
*Western University*, asadrek@uwo.ca

Keyvan Mirbaha

# Characterization of a Carbonate Sand based on Shear Wave Velocity Measurement

Keyvan Mirbaha, & Abouzar Sadrekarimi, Ph.D., P. Eng.
*Department of Civil & Environmental Engineering – Western University, London, ON, Canada*

ABSTRACT
Numerous studies have been carried out on the dynamic behavior of sands. However, few studies have investigated the dynamic characteristics of carbonate sands. This paper presents series of laboratory simple shear tests on specimens of a local carbonate sand from London (ON). Besides monotonic and cyclic shearing, the dynamic behavior of the sand is also characterized by measuring the velocity of shear waves travelling through the specimens. Drained and undrained shearing behavior of specimens with a wide range of relative density and consolidation stresses are tested. Shear wave velocity is found to vary with effective overburden stresses by an average power of 0.25. Maximum shear modulus ($G_{max}$) is also computed from the shear wave velocity measurements and a correlation is developed between $G_{max}$, effective stress, and void ratio for a carbonate sand. The critical state line of the carbonate sand established from the simple shear tests is used for determining the state parameter of each specimen and this is related to the shear wave velocity measured in the same specimen. Such a relationship can be employed for measuring the in-situ state of this carbonate sand. Cyclic resistances of the sand specimens are determined from cyclic shear tests. Combined with shear wave velocity data, these are compared with current liquefaction triggering curves.

## 1 INTRODUCTION

Shear wave velocity ($V_S$) and shear modulus are two of the most fundamental parameters for characterizing materials including soils and play a key role in engineering design practice. $V_S$ is used in several constitutive models to determine the small strain response of soils, to estimate the in-situ stress state of cohesionless soils (Robertson, et al., 1995), ground deformation prediction, for seismic site classification in many design codes, including the current National Building Code of Canada and the Canadian Highway Bridge Design Code, to characterize site-response for evaluating seismic hazard, as well as in assessing the potential for liquefaction triggering of cohesionless soils (Andrus and Stokoe 2000, Clayton, 2011). $V_S$ can be measured both in the laboratory (e.g. using bender elements, or a resonant column device) or in the field by down-hole, cross-hole, suspension logging and surface wave methods. Shear wave velocity ($V_s$) represents soil elasticity and provides a direct measure of the maximum (small-strain) shear modulus ($G_{max}$) of a soil as shown in Equation 1:

$$G_{max} = \rho . V_s^2 \quad [1]$$

Where $G_{max}$ is in Pascal, $V_s$ is in m/s, and ρ is the total soil mass density in kg/m$^3$. Along with soil damping characteristics, $G_{max}$ is a useful parameter for the analysis of natural or man-made structures under dynamic or cyclic loads (e.g., caused by an earthquake, machine foundation, ocean waves, or blast).

Several investigations have been performed on shear wave velocity and shear modulus of cohesionless soils and their correlations with soil characteristics such as relative density and confining pressure (Hardin and Black, 1966, Iwasaki, et al., 1978, Kokusho, 1980, Lo Presti, et al., 1997, Robertson, et al., 1995). These studies have been mostly carried out on sands mainly composed of silica and quartz particles. For example, Hardin and Black (1966) and Robertson, et al. (1995) studied dynamic characteristics of Ottawa sand while Kokusho (1980) focused on the behavior of Toyoura sand. Both of these sands are composed of silica particles.

This paper studies the dynamic behavior of a carbonate sand using bender element measurements and cyclic direct simple shear (DSS) tests. Bender elements provide soil dynamic modulus at very small shear strains (< $10^{-5}$), while cyclic DSS tests are employed to augment $V_S$ measurements from bender elements at higher cyclic shear strains (between 0.1 – 4%). The plane-strain boundary condition and simple shearing mode applied in a DSS test provide a closer representation of in-situ conditions, than a triaxial test. Furthermore, a soil specimen is subjected to repeated abrupt 90$^o$ rotations of principal stresses in a cyclic triaxial test. This is very different than the smooth rotation of principal stress directions which occurs during an actual seismic event or in a cyclic DSS tests.

## 2 EXPERIMENTAL PLAN

### 2.1 Tested Material

A local carbonate-silica sand is tested in the experiments of this study. This sand was collected from Boler Mountain in London, Ontario (called “Boler sand” hereafter). The natural Boler sand contains about 11% fine particles. However, for the experiments of this study the fines were removed in order to focus on the behavior of a clean sand and compare its dynamic behavior with those of other clean sands. A specific gravity ($G_S$) of 2.67, and maximum ($e_{max}$) and minimum ($e_{min}$) void ratios of respectively 0.845 and 0.525 were determined following ASTM standard

procedures. Particle size distribution of Boler sand is presented in Figure 2 with $D_{50}$ = 0.25 mm. Accordingly, Boler sand is classified as a poorly-graded (SP) sand according to the Unified Soil Classification System (USCS). Scanning electron microscopic images, X-Ray diffraction and acid dissolution analyses were carried out to determine particle shape and mineralogy. It was found that the Boler sand is composed of about 90% to 85% quartz ($SiO_2$) and 10% to 15% carbonate ($CaCO_3$) and dolomite ($MgCa(CO_3)_2$) particles, with subangular to angular particle shapes.

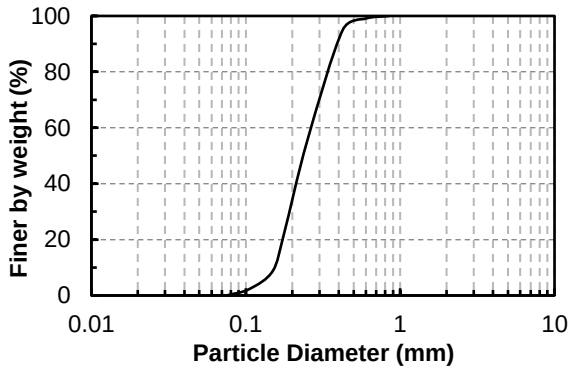


Figure 1. Average grain size distribution of Boler sand

## 2.2 Specimen Preparation

Simple shear tests were carried out using an advanced computer-controlled cyclic simple shear apparatus (Model VDDCSS) manufactured by GDS Instruments (UK). For specimen preparation, a latex membrane was first placed around the bottom cap of the DSS apparatus and secured with an O-ring. Series of 1 mm-thick Teflon-coated stainless steel rings were then stacked around the membrane. Two supporting retainers were used to hold the stacked rings in place during sample preparation and the membrane was then folded over the stacked steel rings. Specimens were prepared at loose ($D_{rc}$ = 25%), medium dense ($D_{rc}$ = 45%), and dense ($D_{rc}$ = 65%) relative densities using the moist tamping method. The height and diameter of the specimens were respectively 20 mm and 70.7 mm in cyclic DSS tests. This corresponds to an aspect ratio of 0.28, which is less than that (0.4) recommended by the ASTM D6528 standard method for simple shear testing.

In regular moist-tamping, the density of the lower sublayers is increased by compacting the overlying layers. This would produce a non-uniform specimen. In order to improve specimen uniformity, the under-compaction (Ladd, 1978) method was used in this study. In this method, over-dried sand was thoroughly mixed with 5% moisture. The specimen was then prepared by compacting moist sand in three sublayers. The first and second sublayers were compacted to dry densities of respectively 5% and 2.5% ("under-compacted") lower than the target dry density of the specimen. After compacting the third overlying sublayer, the final density of these sublayers were hence compacted closer to the target density of the specimen. The dry density was adjusted by changing the mass of soil placed in each sublayer, while all sublayers were compacted to equal heights. Except for the final sublayer, the surface of each sublayer was also scarified in order to improve the bonding between sublayers. The top cap of the DSS apparatus was subsequently lowered on the sand surface, the membrane was folded back on the top cap and then secured with an O-ring. The retainer plates were also removed.

The small amount of moisture content (5%) imparts a small amount of matric suction to a moist-tamped specimen and helps to stabilize the specimen during preparation. However, since this matric suction was not measured here, it was removed by saturating the specimens after specimen preparation. A small seating vertical stress of 5 kPa was first applied to stabilize the specimen and prevent piping. Saturation was then carried out by flushing the specimens with $CO_2$ gas, followed by de-aired water through drainage ports on the specimen endcaps. Carbone dioxide ($CO_2$) was used to enhance specimen saturation as it is heavier than air (so it replaces air during flushing) and it is many times more soluble in water than air. Specimen height was carefully recorded during this process in order to determine the precise initial void ratio of the specimen.

## 2.3 Consolidation

Following saturation, the specimens were consolidated to effective vertical stresses ($\sigma'_{vc}$) of 50, 100, 200, 400, or 600 kPa. The top drainage port was open during consolidation in order to allow excess pore pressure dissipation. Specimens' void ratio after consolidation ($e_c$) was subsequently calculated from changes in specimen height.

## 2.4 Monotonic DSS Tests

Monotonic simple shear tests were carried out in order to determine liquefaction susceptibility and the critical state line of Boler sand. In drained shear tests, a constant effective vertical stress (= $\sigma'_{vc}$) was maintained while changes in specimen height were carefully recorded to determine void ratio changes. Undrained shear was replicated by maintaining a constant specimen volume. This was performed using the electronic feedback and control system of the DSS apparatus by precisely adjusting the vertical stress in order to prevent any volume change during shearing. Volume change resulted from changes in specimen height as the area of the specimen was kept constant by the stainless steel rings. Since pore water pressure was not measured in the DSS apparatus, the top drainage port was left open during shearing. Changes in total vertical stress during constant-volume shear were considered as an equivalent excess pore water pressure which would have developed in an undrained shear test (Dyvik, et al., 1987). Monotonic shearing was carried out at a shear strain rate of 3%/hour up to a shear strain of 30%.

## 2.5 Cyclic DSS tests

Constant-volume cyclic shear tests were carried out to determine the cyclic liquefaction behavior of Boler sand at $\sigma'_{vc}$ = 100 kPa. Similar to the constant-volume monotonic tests, a constant-volume condition was imposed in these

tests by precisely adjusting the vertical stress. Stress-controlled shearing was performed by cycling shear stress within a certain range of stresses at a frequency of 0.1 Hz. Cyclic stress ratio (CSR) is determined as the ratio of the peak shear stress ($\tau_{max}$) to $\sigma'_{vc}$. Tables 1 and 2 summarize the characteristics of the monotonic and cyclic simple shear tests of this study. Note that comparison between particle size distributions before and after testing did not show particle crushing in any of the experimental stages (consolidation, monotonic or cyclic shear)

Table 1. Summary of monotonic DSS tests

| $\sigma'_{vc}$ (kPa) | $e_c$ | $D_{rc}$ (%) | $e_{cs}$ | $\sigma'_{v,cs}$ (kPa) | Drainage |
|---|---|---|---|---|---|
| 100 | 0.762 | 26 | 0.762 | 40.8 | Constant Volume |
| 100 | 0.802 | 13 | 0.802 | 11.3 | |
| 200 | 0.809 | 11 | 0.809 | 19.6 | |
| 300 | 0.778 | 21 | 0.778 | 41.5 | |
| 300 | 0.763 | 26 | 0.763 | 71.8 | |
| 400 | 0.750 | 30 | 0.750 | 86.6 | |
| 800 | 0.728 | 37 | 0.728 | 187 | |
| 1000 | 0.706 | 43 | 0.706 | 346 | |
| 1200 | 0.697 | 46 | 0.697 | 421 | |
| 50 | 0.812 | 10 | 0.782 | 50 | Drained |
| 80 | 0.770 | 23 | 0.758 | 80 | |
| 100 | 0.753 | 29 | 0.753 | 100 | |
| 400 | 0.699 | 46 | 0.697 | 400 | |

Table 2. Summary of Cyclic DSS tests

| CSR | $\tau_{cyc}$ (kPa) | $e_c$ | $D_{rc}$ (%) | $N_L$ |
|---|---|---|---|---|
| 0.066 | 6.6 | 0.770 | 23.4 | 41 |
| 0.080 | 8.0 | 0.759 | 26.4 | 12 |
| 0.090 | 9.0 | 0.764 | 25.2 | 11 |
| 0.065 | 6.5 | 0.700 | 45.2 | 64 |
| 0.075 | 7.5 | 0.706 | 43.4 | 21 |
| 0.085 | 8.5 | 0.700 | 45.2 | 16 |
| 0.075 | 7.5 | 0.638 | 64.8 | 46 |
| 0.090 | 9.0 | 0.634 | 66.0 | 18 |
| 0.100 | 10.0 | 0.634 | 66.0 | 13 |

### 2.6 Shear Wave Velocity Measurement

Shear wave velocity of the specimens were measured by a pair of piezoelectric bender elements embedded with epoxy into the platens of the DSS apparatus. The epoxy-coated bender elements protruded 1 mm into the specimen. Marjanovic and Germaine (2013) show that this bender element setup (shorter and wider tips) produces the best shear waves without significant interference from compression waves. A sinusoidal pulse was applied to the transmitting bender element, which provides high versatility in selecting signal frequency and amplitude (compared to square waves). A high voltage of ±10 Volts was chosen to improve the signal to noise ratio.

Taller specimens of 30 mm high were prepared for measuring shear wave velocity ($V_S$) in order to increase $V_S$ travel distance and improve signal resolution. Shear wave velocity was measured after allowing about 30 minutes of consolidation at $\sigma'_{vc}$. Earlier studies (Lee and Santamarina, 2005, Sanchez-Salinero, et al., 1986, Viggiani and Atkinson, 1995) have often recommended a distance between bender element tips ($L_{tt}$) of at least twice the wavelength ($\lambda$) to reduce near-field effects and allow for the development and propagation of shear waves. Besides preparing taller specimens (= 30 mm), a high frequency (36 kHz) signal was also used to produce short wave lengths and generate at least 2 wavelengths between the bender elements ($L_{tt}/\lambda > 2$). The high signal frequency used in the bender element tests further minimized dispersion from wave reflections at specimen boundaries (Alvarado and Coop 2012).

## 3 RESULTS

### 3.1 Monotonic Shearing Behavior

As shown in Table 1, monotonic shear tests were carried out at wide ranges of consolidation relative density ($D_{rc}$) and $\sigma'_{vc}$. Figure 2 shows effective stress paths for some of the constant-volume monotonic DSS tests. All tests display a significant strain-softening and static liquefaction behavior. A large reduction in $\sigma'_{vc}$ is equivalent to shear-induced pore pressure generation in an undrained condition. Critical state is taken at the minimum shear stress reached after failure, although some tests displayed "phase transformation" (Ishihara, 1993) to a strain-hardening (or dilative) behavior after an extended range of constant volume, shear and effective vertical stresses. An overall frictional angle of $\phi'_{cs}$ = 30° is determined at the critical state from both constant-volume and drained tests. The relatively low $\phi'_{cs}$ is likely associated with the plane-strain boundary condition imposed in DSS testing (Cornforth 1964; Marachi et al. 1981; Terzaghi et al. 1996)

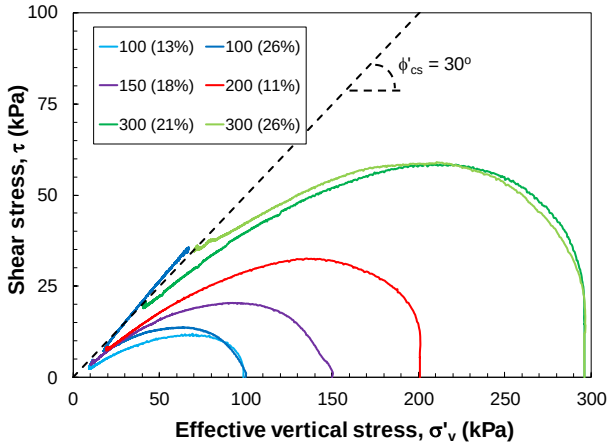


Figure 2. Stress paths for some of the constant-volume monotonic DSS tests

Been and Jefferies (1985) introduced the state parameter ($\psi$) to describe the shearing behavior of a soil based on the combination of void ratio, effective stress and their relation to the critical state void ratio at same effective

stress. The critical state line (CSL) represents a boundary between strain-softening (or contractive) and strain-hardening (or dilative) behaviors of a soil. Table 1 shows void ratio ($e_{cs}$) and effective vertical stress ($\sigma'_{v,cs}$) at the critical state from both drained and constant-volume shear tests. These data are plotted in Figure 3 to establish the CSL for Boler sand as below:

$$e = 0.888 - 0.071\text{Log}(\sigma'_{vc}) \quad [2]$$

This equation suggests a critical void ratio of 0.888 at an effective stress of $\sigma'_{vc}$ = 1 kPa and a critical state line slope of 0.071. CSL of Boler sand is comparable to those for Monterey #0 sand (Jefferies and Been, 2006) and Hokksun sand (Castro, 1969) determined from isotropically-consolidated triaxial compression shear tests. These are compared in Figure 3 assuming a horizontal stress ratio of $K_o$ = 0.5 for converting isotropic effective confining stress (in triaxial tests) to $\sigma'_{vc}$.

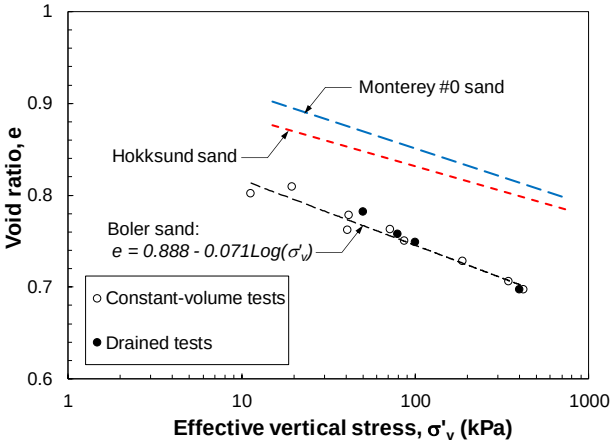


Figure 3. Critical state lines of Boler (from this study), Hokksund (Castro, 1969), and Monterey #0 (Jefferies and Been, 2006) sands

## 3.2 Shear Wave Velocity

Bender elements are piezoelectric cantilever beam-shaped transducers which either bend by an applied voltage or produce a voltage when it is bent. Despite their simple operation, the interpretation of bender element pules can be complicated. While the wave travel distance can be confidently taken as the tip-to-tip distance ($L_{tt}$) between the bender elements (Brignoli, et al., 1996, Viggiani and Atkinson, 1995), identifying the correct travel time is often challenging. Various time and frequency domain methods (Jovicic, et al., 1996, Lee and Santamarina, 2005) are suggested by different researchers to determine travel time.

Figure 4 illustrates the transmitted and received shear waves for some of the experiments. The reverse polarity of the initial small bumps is a characteristic of nearfield effects and compression waves generated from the lateral vibration of the bender elements. These compression-wave signals travel faster and reach the receiving bender element earlier than a shear wave, but rapidly decay in subsequent reflections from the endcaps (Camacho-Tauta, et al., 2015). Low amplitude pulse in the received signal have been observed in other bender-element studies (Arulnathan, et al., 1998, Brandenberg, et al., 2008, Brignoli, et al., 1996), which are often associated with distorted compression waves reflected from the specimen boundaries. These were thus disregarded. The tip-to-tip distance between the bender elements ($L_{tt}$) was measured by subtracting the height of the bender elements from the specimen height.

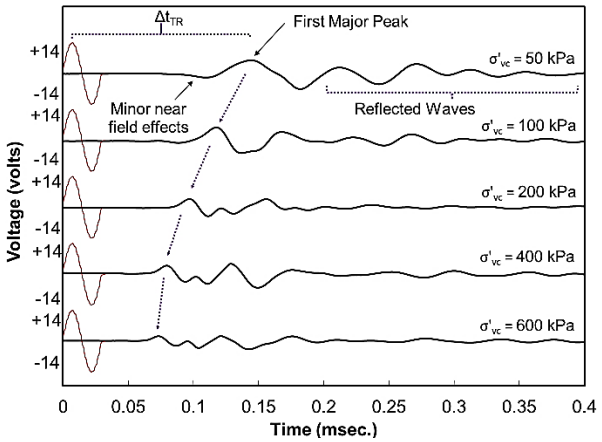


Figure 4. Shear wave signals for $D_{rc}$ = 45% specimen

Similar to Figure 4, almost all the output signals obtained during the present study exhibited a clear major peak (shear-wave). Hence, peak-to-peak time of the first transmitted and received signals was used to measure travel time ($\Delta t_{TR}$) and determine $V_S$. Several investigators suggest that this approach can provide an accurate measurement of $V_S$ (Brignoli, et al., 1996, Camacho-Tauta, et al., 2015, Jovicic, et al., 1996, Lee and Santamarina, 2005, Viggiani and Atkinson, 1995, Yamashita, et al., 2009) which match well with $V_S$ measured by other laboratory techniques (e.g., resonant column tests, acceleration measurements, etc). For example, Yamashita et al. (2009) found that the peak-to-peak time difference between transmitted and received signals provided the most consistent determination of $V_S$ travel time using bender elements among 23 different laboratories around the world. Accordingly, $V_S$ was determined as $\Delta t_{TR}/L_{tt}$. Measurements carried out at higher input frequencies (50 & 83 kHz) results in similar travel times and $V_S$, suggesting that $V_S$ remains unaltered by changes in input frequency.

Shear wave velocity is often expressed as a function of void ratio, F(e) and effective confining pressure ($\sigma'_c$) as below (Hardin and Richart Jr., 1963):

$$V_S\ (m/s) = F(e)\sigma'^{\beta}_c \quad [3]$$

Where exponent $\beta$ is a material constant which reflects the nature of inter-particle contacts (Santamarina, et al., 2001). For the $K_o$-consolidated simple shear samples of this study, $\sigma'_c$ can be approximated as $(1+2K_o)\sigma'_{vc}$.

Because of the difficulties in determining $K_o$ in the field, it is simpler to express $V_S$ as a function of $\sigma'_{vc}$. The influence of effective stress on any soil parameter is usually considered in geotechnical engineering practice by normalization to $\sigma'_{vc}$ = 100 kPa. Similar to the overburden stress correction used for SPT or CPT penetration resistances, Equation 3 is used to account for the effect of overburden pressure on $V_S$. A normalized shear wave velocity ($V_{S1}$) corresponding to $\sigma'_{vc}$ = 100 kPa is often calculated as below:

$$V_{S1} = V_S(P_a/\sigma'_{vc})^{\beta} \quad [4]$$

Where $P_a \approx 100$ kPa. According to Figure 5, irrespective of $D_{rc}$ the typical stress exponent of $\beta = 0.25$ (Hardin and Richart Jr., 1963, Robertson, et al., 1992) fits $V_S$ profile for Boler sand quite well.

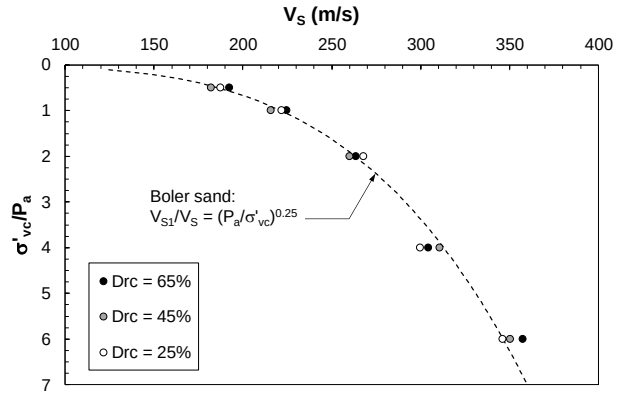


Figure 5. Variation of $V_S$ with normalized effective vertical stress ($\sigma'_{vc}/P_a$) for Boler sand specimens

Several studies (Hardin and Richart Jr., 1963, Robertson, et al., 1995) suggest a linear variation of F(e) with void ratio. As shown in Figure 6, the $V_S$ data of this study also indicate an approximately linear relationship for F(e) which is quite close to the relationship derived by Hardin and Richart Jr. (1963). Figure 6 further suggests a slightly decreasing trend of F(e) and thus $V_S$ with increasing void ratio (similar to Hardin and Richart 1963). Similar to Boler sand, some other studies also report a narrow range of $V_S$ for a wide range of void ratios (Cha, et al., 2014, Santamarina, et al., 2001). According to Figures 5 and 6, Equation 3 is fitted for Boler sand as below:

$$V_S \text{ (m/s)} = (89.4 - 26.6e_c)\sigma'^{0.25}_{vc} \quad [5]$$

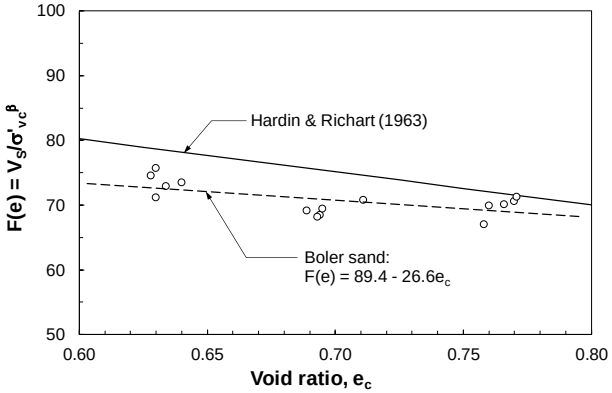


Figure 6. Variation of F(e) with consolidation void ratio ($e_c$) from the experiments of this study for Boler and comparison with the correlation derived by Hardin and Richart (1963)

As both the shearing behavior (e.g. in Fig. 2) and $V_S$ (in Figs. 5 & 6) of Boler sand are affected by $e_c$ and $\sigma'_{vc}$, $V_S$ can be used to determine the liquefaction susceptibility and strain-softening potential of Boler sand.

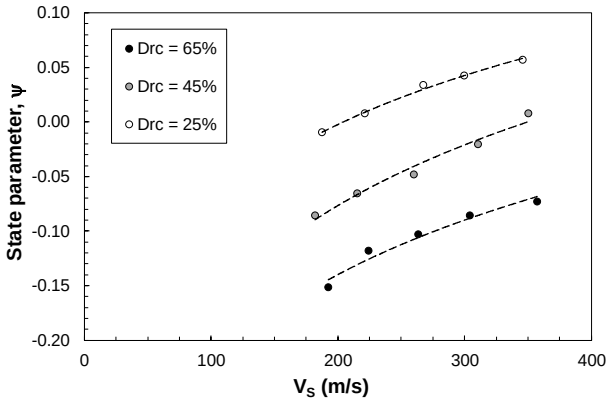


Figure 7: $V_S$ versus state parameter ($\psi$) from the DSS tests of this study

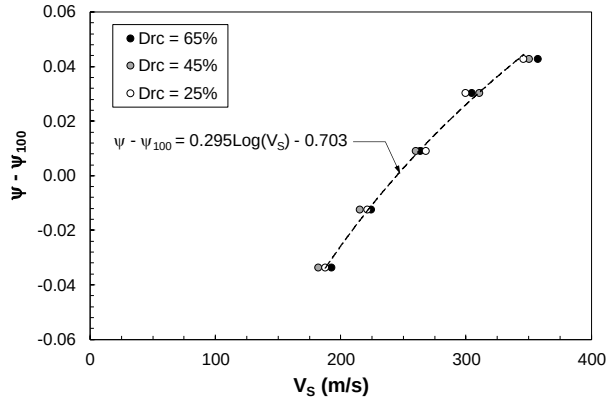


Figure 8. $V_S$ versus ($\psi - \psi_{100}$) from the DSS tests of this study. $\psi_{100}$ is the state parameter at $\sigma'_{vc}$ = 100 kPa

Figures 7 and 8 present the variations in state parameter (determined from Eq. 2) with $V_S$ data for the specimens tested in this study. $\psi_{100}$ is the state parameter calculated at $\sigma'_{vc}$ = 100 kPa. Despite separate relationships between $V_S$ and $\psi$ at different relative densities in Figure 7, a unique trend is found between Vs and $\psi - \psi_{100}$ in Figure 8 regardless of relative densities or stress levels.

### 3.3 Evaluation of Maximum Shear Modulus ($G_{max}$)

As discussed in the Introduction, small-strain or maximum shear modulus of a soil is one of the main purposes of measuring shear wave velocity. $G_{max}$ is a useful and practical parameter for engineering design purposes which correlates soil deformation properties to applied stress. $G_{max}$ is calculated for the specimens of this study using Equation 1.

As shown in Figure 9, $G_{max}$ largely increases with increasing $\sigma'_{vc}$ for a particular $e_c$, whereas the effect of $e_c$ seems to be secondary. It can be explained that increasing $\sigma'_{vc}$ not only raises $\rho$ but also increases stress concentration and friction at particle contacts, resulting in a greater $V_S$ and hence $G_{max}$.

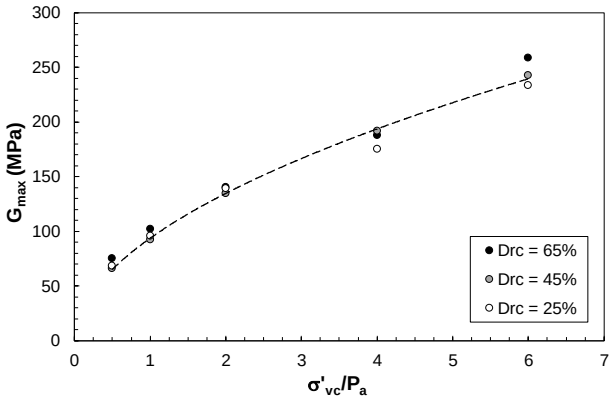


Figure 9. Variation of $G_{max}$ with $\sigma'_{vc}$ for Boler sand at $D_{rc}$ = 25, 45, and 65%

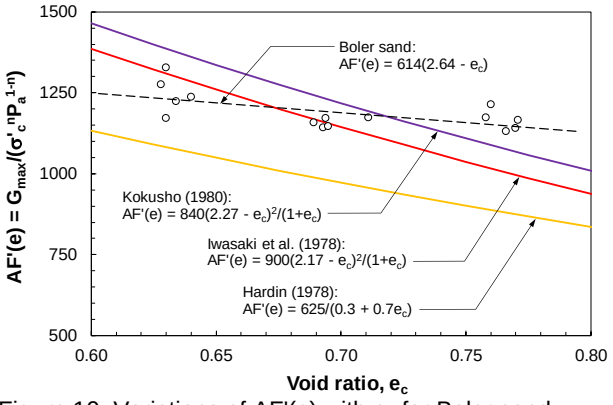


Figure 10. Variations of AF'(e) with $e_c$ for Boler sand tested as well as those suggested by several other studies (Hardin 1978; Iwasaki et al. 1978; Kokusho 1980) for clean sands

Several empirical correlations have been developed for $G_{max}$ characterization, all of which take into account void ratio and effective stress as in the following form (Hardin and Richart Jr., 1963):

$$G_{max}/P_a = AF'(e)(\sigma'_{vc}/P_a)^n \quad [6]$$

Where n is a stress exponent often equal to 0.5 (= 2$\beta$). Equation 6 and in particular F'(e) have been fitted to experimental data by many investigators. Similar to $V_S$, a linear relationship appears to fit F'(e) for the experiments of this study in Figure 10. For the normally-consolidated DSS specimens, $K_o$ = 0.5 is used for converting $\sigma'_{vc}$ to $\sigma'_c$. According to Figure 10, the normalized $G_{max}$ (= $G_{max}/\sigma'^n_c P_a^{1-n}$) data are within the ranges of AF'(e) relationships proposed by several other studies (Hardin, 1978, Iwasaki, et al., 1978, Kokusho, 1980) for clean sands.

### 3.4 Cyclic simple shear tests

Cyclic simple shear tests were carried out to determine the cyclic liquefaction behavior of Boler sand. Figure 11 shows typical results of the cyclic DSS tests of this study. According to this figure, liquefaction is triggered when the equivalent excess pore pressure ratio ($r_u$) – measured as a reduction in vertical stress - exceeds 80%. This corresponded to reaching a double-amplitude cyclic shear strain of 7.5% in the DSS tests. This is essentially equivalent to the liquefaction definition (Vaid and Sivathayalan, 1996) of 5% double-amplitude axial strain in a triaxial test. Liquefaction triggering is followed by much larger increase in cyclic shear strain and loss of shear stiffness in Figure 11.

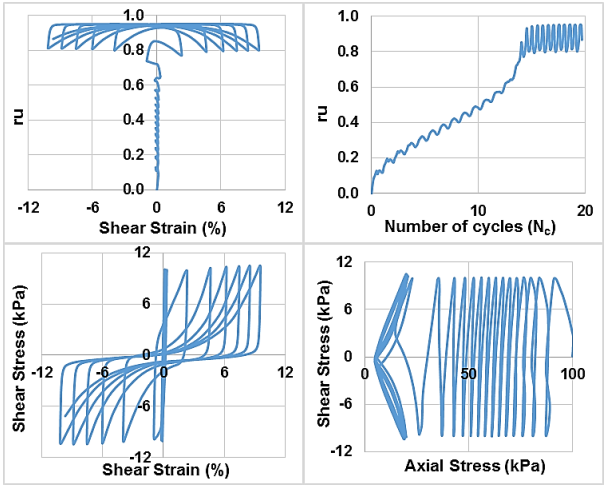


Figure 11. Cyclic DSS test results on a Boler sand specimen at $D_{rc}$ = 65%, $\sigma'_{vc}$ = 100 kPa and CSR=0.100

The cyclic stress ratio (=$\tau_{cyc}/\sigma'_{vc}$) required for liquefaction occurrence in a specified number of loading

cycles is called “Cyclic Resistance Ratio (CRR)”. Figure 12 shows the number of cycles to triggering liquefaction ($N_L$) at different CSR for specimens consolidated to $\sigma'_{vc}$ = 100 kPa. For an earthquake magnitude of 7.5, CRR is defined as the CSR to cause liquefaction in 15 uniform cycles of shear stress (Seed and Idriss, 1971).

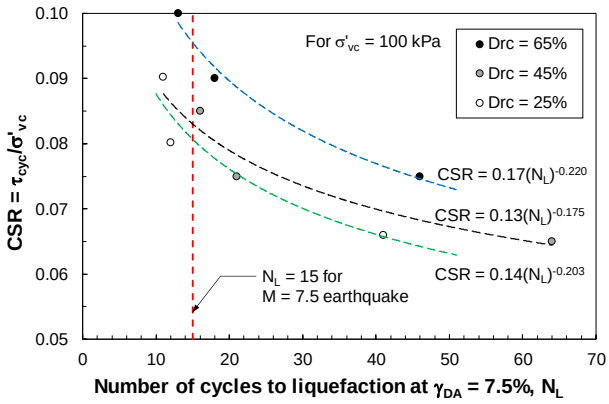


Figure 12. CSR versus number of cycles ($N_L$) to trigger liquefaction for Boler sand at $\sigma'_{vc}$ = 100 kPa

In the simplified stress-based approach for liquefaction analysis, seismic demand is calculated as the cyclic shear stress ratio applied by an earthquake (CSR) and the cyclic resistance ratio (CRR) of the soil (capacity) is estimated from a correlation with an in-situ test. Earthquake-induced CSR can be estimated using the Seed and Idriss (1971) simplified procedure or numerical methods such as finite element method based seismic response analysis. The simplified procedure provides CRR of a level-ground (no shear stress bias) for an effective overburden pressure of 100 kPa. Cyclic liquefaction is deemed to occur when CSR exceeds CRR. Semi-empirical relationships between CRR and SPT or CPT penetration resistance have been extensively studied by many researchers. Determining CRR from in-situ shear wave velocity measurement can be a particularly useful alternative for sites underlain by soils that are difficult to penetrate or extract undisturbed samples. Robertson, et al. (1992) present one of the earliest boundary curves between liquefaction and non-liquefaction cases using a limited field database. Based on cases of liquefaction and non-liquefaction for 26 earthquakes and more than 70 different sites, Andrus and Stokoe (2000) developed relationships between CRR and $V_{S1}$ which are the current state of practice for evaluating liquefaction potential using $V_{S1}$.

Pairs of shear wave velocity ($V_{S1}$) and $CRR_1$ measured from the experiments of this study at $\sigma'_{vc}$ = 100 kPa are compared with these $V_S$-based liquefaction trigging boundaries in Figure 13. As illustrated in this figure, Bolder sand exhibits lower liquefaction resistance than the field-based liquefaction triggering curves. In other words, the current methods for estimating liquefaction resistance could largely overestimate CRR of Boler sand. This would lead to an unsafe liquefaction analysis. The lower CRR of Boler sand compared to that from field-based CRR curves is possibly associated with the carbonaceous composition of Boler sand as well as differences in the triggering of liquefaction in the laboratory and in the field. Because of the effects of excess pore pressure redistribution and upward flow of water, the triggering of cyclic liquefaction could occur at much smaller cyclic shear strains (≈ 0.06 – 0.12%) in the field (Dobry, et al., 2015). Whereas, liquefaction is determined at a single-amplitude shear strain of 3.75% in laboratory DSS tests.

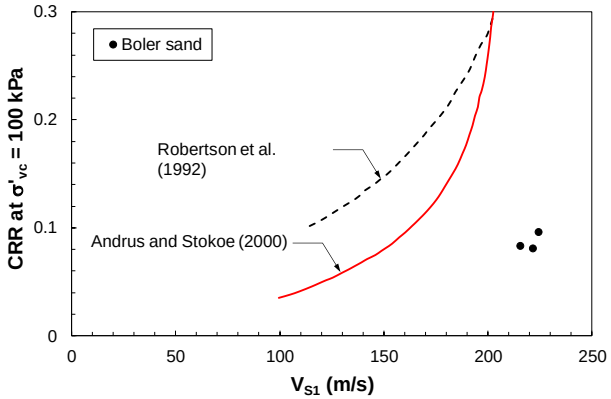


Figure 13. Comparison of $CRR_1$ (at $\sigma'_{vc}$ = 100 kPa) and $V_{S1}$ for Boler sand with liquefaction triggering curves of Andrus and Stokoe (2000) and Robertson et al. (1992)

## 4 CONCLUSIONS

This paper presented the monotonic and cyclic behavior of a carbonate sand (“Boler sand”) from London Ontario. Shear wave velocity ($V_S$) and small-strain stiffness ($G_{max}$) were also measured using bender element tests. Power functions were used to fit $V_S$ and $G_{max}$ data with effective vertical stress with exponents of 0.25 and 0.50, respectively. Both $V_S$ and $G_{max}$ however displayed a much weaker variation with void ratio. Despite the weak effect, linear functions were used to describe the effect of void ratio on $V_S$ and $G_{max}$. The critical state line of Boler sand, determined from the monotonic shear tests, was found to be similar to those of some other clean sands. State parameters ($\psi$) of the specimens were subsequently calculated using the critical state line and initial states of the specimens. Separate relationships were found between $\psi$ and $V_S$ at different relative densities, suggesting that $\psi$ is not a suitable parameter to combine the effects of void ratio and effective stress on $V_S$. Cyclic liquefaction behavior of Boler sand was also determined from cyclic DSS tests. It was found that the current liquefaction triggering method could significantly overestimate the liquefaction resistance of Boler sand, leading to unsafe liquefaction analysis. This could be associated with the carbonaceous composition of Boler sand as well as differences in the triggering of liquefaction in the laboratory and in the field.

## 5 REFERENCES


Andrus, R. D., and Stokoe, K. H. (2000). "Liquefaction resistance of soils from shear-wave velocity." *Journal of Geotechnical and Geoenvironmental Engineering*, 126(11): 1015-1025.

Arulnathan, R., Boulanger, R. W., and Riemer, M. F. (1998). "Analysis of bender element tests." *Geotechnical Testing Journal, ASTM*, 21(2): 120 - 131.

Brandenberg, S. J., Kutter, B. L., and Wilson, D. W. (2008). "Fast stacking and phase corrections of shear wave signals in a noisy environment." *Journal of Geotechnical and Geoenvironmental Engineering*, 134(8): 1154-1165.

Brignoli, E. G. M., Gotti, M., and Stokoe II, K. H. (1996). "Measurement of shear waves in laboratory specimens by means of piezoelectric transducers." *Geotechnical Testing Journal, ASTM*, 19(4): 384 - 397.

Camacho-Tauta, J., Cascante, G., Fonseca, V. D., and Santos, J. (2015). "Time and frequency domain evaluation of bender element systems." *Geotechnique*, 65(7): 548 - 562.

Castro, G. (1969). "Liquefaction of sands." Ph.D., Harvard University, Cambridge, Massachusetts.

Cha, M., Santamarina, J., Kim, H., and Cho, G. (2014). "Small-strain stiffness, shear-wave velocity, and soil compressibility." *Journal of Geotechnical and Geoenvironmental Engineering, ASCE*, 140(10).

Clayton, C. R. I. (2011). "Stiffness at small strain: research and practice." *Geotechnique*, 61(1): 5 - 37.

Cornforth, D. H. (1964) “Some experiments on the influence of strain conditions on the strength of sand.” *Geotechnique*, 14:143–167

Dobry, R., Abdoun, T., Stokoe II, K. H., Moss, R. E. S., Hatton, M., and El Ganainy, H. (2015). "Liquefaction potential of recent fills versus natural sands located in high-seismicity regions using shear-wave velocity." *Journal of Geotechnical and Geoenvironmental Engineering, ASCE*, 141(3): 1 - 13.

Dyvik, R., Berre, T., Lacasse, S., and Raadim, B. (1987). "Comparison of truly undrained and constant volume direct simple shear tests." *Geotechnique*, 37(1): 3 - 10.

Hardin, B. O. (1978). "The nature of stress-strain behavior of soils." *ASCE Geotechnical Engineering Division Speciality Conference on Earthquake Engineering and Soil Dynamics*, Pasadena, California, pp. 3 - 90.

Hardin, B. O., and Black, W. L. (1966). "Sand stiffness under various triaxial stresses." *Journal of the Soil Mechanics and Foundations Division, ASCE*, 92(2): 27 - 42.

Hardin, B. O., and Richart Jr., F. E. (1963). "Elastic wave velocities in granular soils." *Journal of Soil Mechanics and Foundation Division, American Society of Civil Engineers*, 89(1): 33 - 65.

Ishihara, K. (1993). "Liquefaction and flow failure during earthquakes." *Geotechnique*, 43(3): 351 - 415.

Iwasaki, T., Tatsuoka, F., and Takagi, Y. (1978). "Shear moduli of sands under cyclic torsional shear loading." *Soils and Foundations*, 18(1): 39 - 56.

Jefferies, M. G., and Been, K. (2006). *Soil liquefaction - a critical state approach*, Taylor & Francis, New York.

Jovicic, V., Coop, M. R., and Simic, M. (1996). "Objective criteria for determining Gmax from bender element tests." *Geotechnique*, 46(2): 357 - 362.

Kokusho, T. (1980). "Cyclic triaxial test of dynamic soil properties for wide strain range." *Soils and Foundations*, 20(2): 45-60.

Ladd, R. S. (1978). "Preparing test specimen using undercompacton." *Geotechnical Testing Journal, ASTM*, 1(1): 16 - 23.

Lee, J.-S., and Santamarina, J. C. (2005). "Bender elements: performance and signal interpretation." *Journal of Geotechnical and Geoenvironmental Engineering, ASCE*, 131(9): 1063 - 1070.

Lo Presti, D. C. F., Jamiolkowshi, M., Pallara, O., Cavallaro, A., and Pedroni, S. (1997). "Shear modulus and damping of soils." *Geotechnique Symposium in Print*, 43(3): 603 - 617.

Marachi, N., Duncan, J., Chan, C., and Seed, H. (1981). “Plane-strain testing of sand.” In: Yong RN, Townsend FC (eds) *Laboratory shear strength of soils*, ASTM STP 740. American Society for Testing and Materials, pp 294–302

Marjanovic, J., and Germaine, J. T. (2013). "Experimental study investigating the effects of setup conditions on bender element velocity results." *Geotechnical Testing Journal, ASTM*, 36(2): 1 - 11.

Robertson, P. K., Sasitharan, S., Cunning, J. C., and Sego, D. C. (1995). "Shear-wave velocity to evaluate in-situ state of Ottawa sand. ." *Journal of Geotechnical Engineering, ASCE*, 121(3): 262 - 273.

Robertson, P. K., Woeller, D. J., and Finn, W. D. L. (1992). "Seismic Cone Penetration Test for Evaluating Liquefaction Potential under Cyclic Loading." *Canadian Geotechnical Journal*, 29(4): 686-695.

Sanchez-Salinero, I., Roesset, J. M., and Stokoe, I. I. (1986). "Analytical studies of body wave propagation and attenuation.", University of Texas, Geotechnical Engineering Center, Texas, Austin.

Santamarina, J. C., Klein, K. A., and Fam, M. A. (2001). *Soils and Waves: Particulate Materials Behavior, Characterization and Process Monitoring*, Wiley, New York.

Seed, H. B., and Idriss, I. M. (1971). "Simplified procedure for evaluating soil liquefaction potential." *Journal of the Soil Mechanics and Foundations Division, ASCE*, 97(SM9): 1249 - 1273.

Terzaghi, K., Peck, R. B., and Mesri, G. (1996). *Soil mechanics in engineering practice*, 3rd edn. Wiley, New York

Vaid, Y. P., and Sivathayalan, S. (1996). "Static and cyclic liquefaction potential of Fraser River delta sand in simple shear and triaxial tests." *Canadian Geotechnical Journal*, 33(2): 281 - 289.

Viggiani, G., and Atkinson, J. H. (1995). "Interpretation of bender element tests." *Geotechnique*, 45(1): 149 - 154.

Yamashita, S., Kawaguchi, T., Nakata, Y., Mikami, T., Fujiwara, T., and Shibuya, S. (2009). "Interpretation of International Parallel Test on the Measurement of G(Max) Using Bender Elements." *Soils and Foundations*, 49(4): 631-650.